Monitoring Soil Salinization in Manas River Basin, Northwestern China Based on Multi-spectral Index Group

Xiaoyan Shi (1,2), Jianghui Song (1,2), Haijiang Wang (1,2), Xin Lv (1,2)

[1]College of Agriculture, Shihezi University, Shihezi 832000, Peoples R China
[2]The Key Laboratory of Oasis Ecological Agriculture of Xinjiang Production and Construction Group, Shihezi University, Shihezi, Xinjiang 832003, Peoples R China
Email: SXYEDU@163.com; SongJH0325@163.com; wanghaijiang@shzu.edu.cn; lxshz@126.com

KEY WORDS: Soil salinization, Spectral-index group, Data transformation, Model, Soil salinity monitoring

ABSTRACT: Large-scale and accurate monitoring soil salinization is essential for controlling soil degradation and sustainable agricultural development. The agricultural irrigation area of the Manas River Basin in the arid area of Northwest China was selected as the test area. 337 soil samples of different land use types in the study area were collected, combined with 11 bands of Landsat images and 17 spectral indices of plant, soil and water. The soil salinization monitoring model based on spectral index group was constructed by comparing the accuracy of principal component regression (PCR), partial least squares regression (PLSR) and multiple linear regression (MLR) models using the transformation of multi-spectral index group and index screening. The results showed that there was a certain correlation between the 28 spectral index groups, with a maximum correlation coefficient -0.3689 between the original spectral group and the soil salt content was B10 band. After the transformation of original data for the logarithm Ln(R), exponential e^R and square root $R^{1/2}$ respectively, the correlation between each index and soil salinity was significantly improved, with the maximum correlation coefficient was up to -0.7564 of $R^{1/2}$. The salt content estimation models were constructed by different data transformation using PLSR, PCR and MLR methods, respectively. This study provides a fast and accurate method for monitoring regional soil salinity content and the results can provide a reference for soil salinity grading management in arid and semi-arid areas.

1. Introduction

Soil salinization is a typical soil degradation phenomenon occurring in arid and semi-arid regions (Metternicht and Zinck, 2003; Fernandez-Buces et al., 2006；Wang et al., 2012). At present, global salinized soil accounts for about 3% of global land resources, which increases by 2.0×10^6 hm^2 per year (Peng et al., 2019). Secondary salinization area is about 7700 hm^2, 58% of which occurs in irrigated agricultural areas (Metternicht and Zinck, 2003). Due to the high soluble salt content of soil parent material, low rainfall, high evaporation intensity, shallow groundwater burial depth and unreasonable water resources management, soil salinization is increasingly severe in arid and semi-arid areas (Shrivastava et al., 2015). The total area of saline soil in China has currently reached 36 million hectares, of which, saline soil in cultivated land accounts for 6.62% (The

National Soil Survey Office, 1998). Salinized soil not only changes the physicochemical properties of the soil, but also inhibits crop growth in severe cases (Wang et al., 2015). Accordingly, rapid and accurate acquisition of regional soil salinity dynamics is a prerequisite for better utilization of salinized farmland.

In summary, current inversion of soil salinity by remote sensing technology is mainly to build salt content estimation model based on salt-sensitive spectral band or in combination with simple spectral index. Studies on optimization, evaluation principles of the model construction index as well as comprehensive estimation accuracy of multi-type spectral indexes are still insufficient (Jibo et al., 2018; Hao et al., 2018). Therefore, taking saline-alkali soil in Manas River Basin in Xinjiang, China as the research object, based on extensive situ measurement of soil salt samples, this study integrates Landsat 8 remote sensing data and vegetation, soil and water spectral index groups, comparatively analyzes the impact of spectral data transformation, spectral index screening group on accuracy of soil salinity inversion model using principal component regression, partial least squares regression and multiple linear regression. A quantitative estimation model of soil salinity is constructed, accuracy of the salt content inversion model is assessed under different model input variables and different model methods to provide a reference for quantitative inversion of salinity by remote sensing in arid and semi-arid regions.

2. Materials and methods

2.1 Overview of the study area

Manas River Basin, located in Xinjiang, China, is adjacent to Tianshan Mountains in the north and Junggar Basin in the south. The basin is located in the hinterland of Eurasia, with an average annual temperature of 4-7°C. It is hot in summer and cold in winter. The precipitation varies greatly in time and space, with average annual precipitation at 110-200 mm and annual average evaporation at 1500-2100 mm. The geomorphology of the Manas Basin has a typical mountain basin system structure, which is mountainous area-piedmont plain-desert in turn (Shao & Cui, 2003). After the river developed in the southern mountainous region enters the basin, the soil carried by it gradually deposits, forming alluvial flood fans, impact plains, and dry deltas in this order. Affected by factors such as regional soil parent material, groundwater level, and climatic conditions, a large number of different types of saline soils are distributed in the area, especially the alluvial fan edges and flood plain with high groundwater level, abundant groundwater volume, and poor flow, which cause severe salinization in the top part of the alluvial plain (Wang et al., 2010).

2.2 Field data acquisition and processing

In this study, a field sampling survey was carried out on Manas River Basin from July to August 2017. The layout of the samples gave comprehensive considerations to different land use types, planting structures, landform types, irrigation methods and soil types. A total of 337 observation sample regions were set in sampling points with wide coverage, representativeness and diverse terrain types (Figure 1). GPS was used to accurately locate and record coordinates of each sampling point. Each plot area is about 30 m×30 m (corresponding to single pixel area in Landsat image). In each sample area, 5 soil surface samples (0-20 cm) were collected by five-point

sampling method, uniformly mixed to form a mixed soil sample and brought back to the laboratory. After drying, sieving and grinding, the samples were screened through 2 mm sieve. Total salt content of the soil was determined by gravimetric method with a 1:5 soil-to-water solution (BAO, 2010). A total of 337 samples were randomly divided into two groups, of which 253 were used for modeling (75% of the samples) and 84 samples were used for verification.

Table 1 Descriptive statistical analysis table of soil sample salt content

Sample（number）	Mean（g kg^{-1}）	Max（g kg^{-1}）	Min（g kg^{-1}）	SD（g kg^{-1}）	CV（%）
Calibration data set（253）	15.67	35.29	0.38	7.26	46.33
Validation data set（84）	17.56	34.28	0.30	7.39	42.08
Total sampling points（337）	16.14	35.29	0.30	7.32	45.35

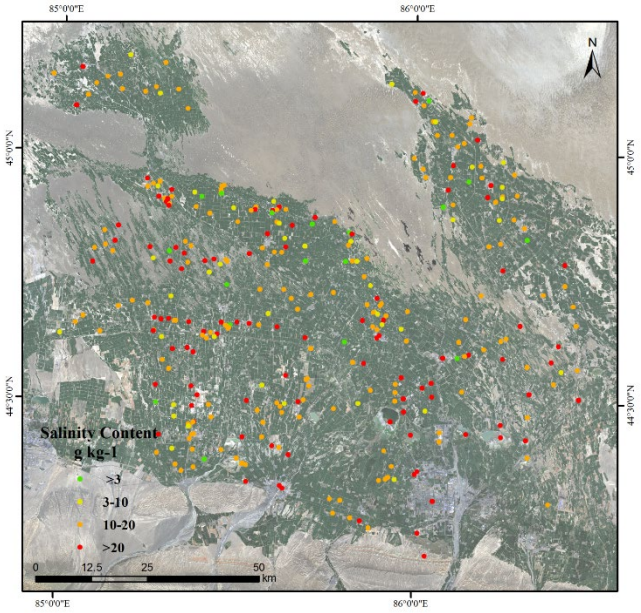

Figure 1 distribution map soil salinity at sampling points in the test area

2.3 Image data processing and index selection

The selection of remote sensing image data was basically consistent with field sampling of soil in time. The Landsat 8 remote sensing image of the Manas River Basin in Xinjiang, China on July 13, 2017 was collected (www.gscloud.cn/). The projected coordinate system is UTM-WGS84, with a total of 11 bands (B). The image preprocessing work of geometric correction, radiation calibration and FLAASH atmospheric correction was carried out using ENVI 5.3 software, and the surface reflectance value of each band corresponding to the field sampling points was extracted. Spectral index can magnify weak connection between the amplification bands, reduce model complexity and remove redundant variables (Shi, 2014). Many researchers have tried to introduce it into remote sensing inversion model to improve estimation accuracy of the model (Allbed et al., 2014; Kertész & Tóth, 1994). After consulting domestic and foreign literatures, 17 spectral indexes related to soil salinity inversion were selected as analysis indexes, including 5 vegetation indexes (V), 11 soil indexes (S) and 1 water body index (W) (Table 2).

Table 2 Spectral index and formula

Salinity Indices	Full name	Spectral Functions	Reference
NDVI	Normalized difference vegetation index	$\mathrm{NDVI} = （\rho_{NIR} - \rho_R）/(\rho_{NIR} + \rho_R)$	Rouse (1973)
GDVI	Generalized Difference Vegetation Index	$\mathrm{GDVI} = (\rho_{NIR}^n - \rho_R^n)/(\rho_{NIR}^n + \rho_R^n)$	Sripada et al. (2006)
WDVI	Weighted difference vegetation index	$\mathrm{WDVI} = \rho_{NIR} - \mathrm{a} \times \rho_R$	Basso et al. (2000)
SAVI	Soil Adjusted Vegetation Index	$\mathrm{SAVI} = \frac{(\rho_{NIR} - \rho_R)}{\rho_{NIR} + \rho_R + L} \times (1 + L), L = 0.5$	Huete (1988)
RVI	Ratio vegetation index	$\mathrm{RVI} = \rho_R/\rho_{NIR}$	Pearson et al. (1972)
NDSI	Normalized difference salinity index	$\mathrm{NDSI} = (\rho_R - \rho_{NIR})/(\rho_R + \rho_{NIR})$	Tripathi et al. (1997)
SI	Salinity Index	$\mathrm{SI} = \sqrt{\rho_B + \rho_R}$	Tripathi et al. (1997)
SI1	Salinity Index 1	$\mathrm{SI1} = \sqrt{\rho_B + \rho_G}$	Khan et al. (2005)
SI2	Salinity Index 2	$\mathrm{SI2} = \sqrt{\rho_{G^2} + \rho_{R^2} + \rho_{NIR^2}}$	Douaoui et al. (2006)
SI3	Salinity Index 3	$\mathrm{SI3} = \sqrt{\rho_{R^2} + \rho_{G^2}}$	Douaoui et al. (2006)
S1	Salinity Index	$\mathrm{S1} = \rho_B/\rho_R$	Bannari et al. (2008)
S2	Salinity Index	$\mathrm{S2} = (\rho_B - \rho_R)/(\rho_B + \rho_R)$	Bannari et al. (2008)
S3	Salinity Index	$\mathrm{S3} = (\rho_G \times \rho_R)/\rho_B$	Bannari et al. (2008)
S5	Salinity Index	$\mathrm{S5} = (\rho_B \times \rho_R)/\rho_G$	Khan et al. (2007)
S6	Salinity Index	$\mathrm{S6} = (\rho_{NIR} \times \rho_R)/\rho_G$	Khan et al. (2007)
SI-T	Salinity Index	$\mathrm{SI-T} = \rho_R/\rho_{NIR} \times 100$	Tripathi et al. (1997)
LSWI	Land Surface Water Index	$\mathrm{LSWI} = (\rho_{NIR} - \rho_{SWIR})/(\rho_{NIR} + \rho_{SWIR})$	Nield et al. (2007)

2.4 Remote Sensing Inversion Model of Soil Salt

In order to find the relationship between the selected indexes and soil salinity, all remote sensing indexes were subject to mathematical transformation. There will be errors in remote sensing images due to lighting conditions and terrain factors, and mathematical transformation can lower the impact of noise on spectrum to a certain extent, thereby strengthening the relationship between remote sensing indexes and soil salinity. To further analyze the relationship between soil remote sensing index and soil salinity, the soil salt content data of each sampling point and the standardized soil remote sensing index (indicated by R) were mathematically transformed, and the transformation forms include reciprocal (1/R), exponent (e^R), logarithm (Ln(R)), reciprocal of logarithm (1/ln(R)), reciprocal of exponent ($1/e^R$), root mean square ($R^{1/2}$). All the indexes were standardized using the formula as follows:

$$\mathrm{x}' = (\mathrm{x} - \mathrm{x}_{\min})/(\mathrm{x}_{\max} - \mathrm{x}_{\min})$$

Whereas x is an original value, x′ is the normalized value.

For the selection of sensitive bands for remote sensing modeling of soil salinity, soil salinity content and all indexes under each transformation are usually selected for correlation analysis. At present, remote sensing technology mainly adopts regression model for inversion of soil salinity. In this study, principal component regression (PCR), partial least squares regression (PLSR) and multiple linear regression (MLR) modeling methods were selected for remote sensing inversion of soil salinity. The accuracy of the salt interpretation model was tested by cross-validation, and the optimal model was selected by comparing accuracy and reliability of the model based on the determination coefficient of the test model, the root mean square error value. For higher R^2(V), the stability and fitting degree of the model is higher; for lower RMSE(V), the model has better estimation capacity.

$$R^2(C)=1-\frac{\sum_{i=1}^{n_c}(y_{ci}-\hat{y}_{ci})^2}{\sum_{i=1}^{n_c}(y_{ci}-\bar{y}_{ci})^2} \qquad R^2(V)=1-\frac{\sum_{i=1}^{n_p}(y_{pi}-\hat{y}_{pi})^2}{\sum_{i=1}^{n_p}(y_{pi}-\bar{y}_{pi})^2}$$

$$RMSE(C)=\sqrt{\frac{1}{n}\sum_{i=1}^{n_c}(y_{ci}-\hat{y}_{ci})^2} \qquad RMSE(V)=\sqrt{\frac{1}{n}\sum_{i=1}^{n_p}(y_{pi}-\hat{y}_{pi})^2}$$

where y_i is the observed value, $\hat{y}_i$ is the interpreted value, $\bar{y}_i$ is the mean value, and n is the number of data points. C represents for calibration and P represents for validation.

3 Result analysis

3.1 Correlation between soil salinity and band, spectral index

In order to understand the sensitivity of different remote sensing bands to soil salinity, the correlation between soil salinity in the study area and the original band reflectance of Landsat was analyzed. Except B6 and B8 bands (whose correlation coefficients are 0.094, -0.058, respectively), indexes of other bands have a significant correlation with salt, and the largest relevant B10 band has a correlation coefficient of 0.3689, which is consistent with the results of Peñuelas (1997). Soil salt is significantly negatively correlated with B10 and B11 bands, with correlation coefficients r of -0.369 and -0.359, respectively. A significant correlation is shown between soil salt content and salinity index, vegetation index. Where, the correlation coefficient between SI2 and salt content is -0.3129, and the correlation coefficients of RVI, NDVI, WDVI and SAVI are -0.3027, -0.3078, -0.3143 and -0.3112, respectively. Each vegetation index shows a significant negative correlation, which is probably because the sampling time is July when the surface has different degrees of vegetation coverage, if the soil salt content exceeds a certain value, plant growth will be inhibited, leading to increased reflectance of red light band and decreased reflectance of near-infrared band, thereby affecting the associated vegetation index.

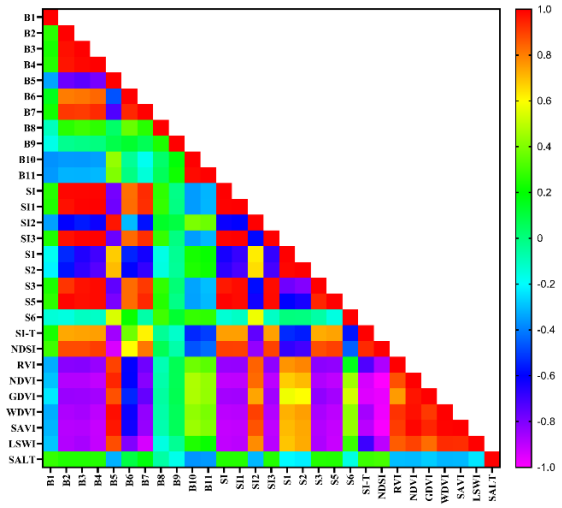

Figure 2 Correlation heat map between original index and soil salinity

Figure 3 shows the correlation coefficient between each index and salt content after 1/Ln(R), $1/e^R$, 1/R, Ln(R), e^R and $R^{1/2}$ transformation of the original data. It can be seen that 1/Ln(R), $1/e^R$, 1/R data transformations fail to significantly increase the correlation between each index and salt, but after logarithmic transformation Ln(R), exponential transformation e^R and square root transformation $R^{1/2}$, the correlation between each index and soil salinity is significantly improved. Where, Ln(R) and e^R transformations can significantly improve the positive correlation with B5, SI2, S1, S2, RVI, NDVI, GDVI, WDVI, SAVI and LSWI, and improve negative correlation with B2, SI,SI1,SI3,S3,S5,SI-T and NDSI; R1/2 transformation can improve positive correlation with B1, B2, B3, B4, B6, B7, SI, SI1, SI3, S3, S5, SI-T and NDSI, and improve negative correlation with B5, B10, B11, SI2, S1, S2, S6, RVI, NDVI, GDVI, WDVI, SAVI and LSWI. The vegetation index in each transformation is negatively correlated to the salt index, which also indicates that the vegetation index decreases as soil salinity increases.

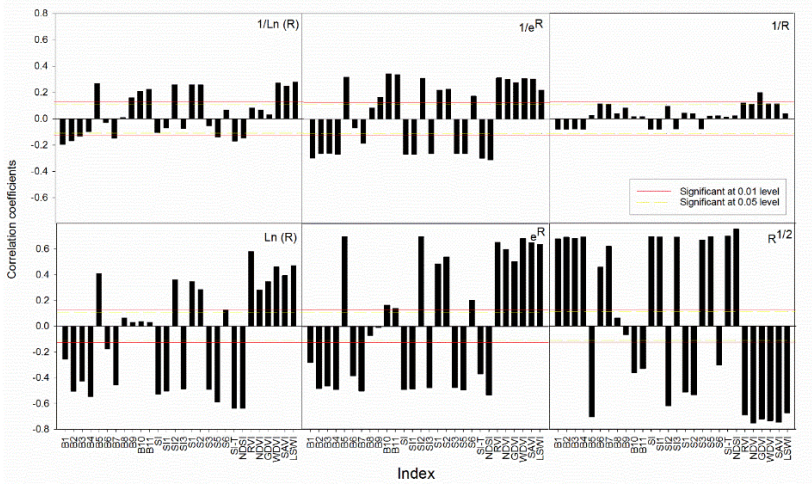

Figure 3 Correlation coefficient map of different index and soil salt content after 6 transformation

Note: R represents normalized variables.

3.2 Construction of soil salinity interpretation model

3.2.1 Estimation accuracy of different data transformation models

The soil salt content estimation model was constructed by PLSR, PCR and MLR methods respectively, and the effect of different data transformations on the accuracy of the estimation model was compared and analyzed (Table 3). Seen from determination coefficient and root mean square error of the model, after e^R, $1/e^R$, Ln(R), 1/Ln(R) and $R^{1/2}$ transformations of the original spectrum, determination coefficient R^2(C), root mean square error RMSE(C) of the modeling set, plus determination coefficient R^2(V), root mean square error RMSE(V) of the prediction set are significantly improved. After e^R,1/ e^R, Ln(R), 1/Ln(R), $R^{1/2}$ transformations, PLSR method-based modeling set R^2(C) are 0.6347, 0.5899, 0.6083, 0.5752 and 0.6489, respectively, and RMSE(C) are 4.4924, 5.1904, 4.6521, 5.2503 and 4.0345 g kg^{-1}, respectively. PLSR method has superior estimation accuracy than PCR and MLR methods, indicating that data transformation through spectral indexes has certain effect on improving accuracy and stability in soil salt content prediction. The inversion accuracy of five mathematical transformation forms is comprehensively compared. R1/2 transformation model has more significant modeling and prediction effects than

models eR, $1/e^R$, Ln(R) and 1/Ln(R), and R^2 of the modeling set and the prediction set are 0.6489 and 0.6033, respectively, while RMSE are 4.0345 and 4.5456 g kg^{-1}, respectively, suggesting that $R^{1/2}$ transformation can better eliminate the effect of natural factors such as soil texture and soil parent material as well as human factors on spectral index, thus enhancing accuracy of spectral index in estimating soil salt content.

Table 3 Estimation accuracy of different data transformation

Data Transformation	PLSR				PCR				MLR			
	R^2(C)	RMSE(C) (g kg^{-1})	R^2(V)	RMSE(V) (g kg^{-1})	R^2(C)	RMSE(C) (g kg^{-1})	R^2(V)	RMSE(V) (g kg^{-1})	R^2(C)	RMSE(C) (g kg^{-1})	R^2(V)	RMSE(V) (g kg^{-1})
R	0.4749	5.0811	0.2487	8.1683	0.3511	7.0081	0.2204	8.198	0.3048	6.8841	0.1039	11.8955
1/R	0.3283	6.1599	0.2318	8.0962	0.3057	7.0107	0.2611	8.0687	0.2961	7.0022	0.1251	10.0285
e^R	0.6347	4.4924	0.4249	5.0514	0.5339	5.0748	0.4446	5.4958	0.5021	4.8623	0.1532	9.6235
$1/e^R$	0.5899	5.1904	0.459	6.0092	0.5065	4.9259	0.3978	6.0883	0.4964	4.9759	0.355	7.4023
Ln(R)	0.6083	4.6521	0.1904	5.9934	0.4647	5.4385	0.3785	6.2766	0.4632	5.1374	0.2497	8.2145
1/Ln(R)	0.5752	5.2503	0.4154	6.2463	0.5106	4.9051	0.4207	5.8406	0.4806	5.3569	0.329	7.9767
$R^{1/2}$	0.6498	4.0345	0.6033	4.5456	0.5634	4.6333	0.5237	5.0075	0.5281	4.6079	0.3983	7.0101

3.2.2 Calibration index and accuracy of model

In the study, 28 spectral group indexes were selected and added to the model from big to small according to absolute values of correlation, so that the relationship between the number of screening index factors and equation determination coefficient as well as equation prediction accuracy was obtained. Figure 4 shows accuracy verification of the PLSR model when different variables are selected under different data transformation. When the number of factors participating in the modeling increases gradually, except 1/R transformation form, the other six transformation forms show consistent variation trend in model verification accuracy. That is, as the number of model factors increases, model stability increases first and then decreases, while fitting performance of 1/R transform processing model increases with the increase of index factor, reaching optimal state when all factors participate in the modeling (R^2(V) and RMSE(V) are 0.2318 and 8.0962 g kg^{-1}, respectively). Seen from determination coefficient of soil salinity and prediction accuracy, except 1/R and Ln(R), the soil salt monitoring models of other transformations are superior to the original spectral modeling results, indicating that certain data transformation of the original spectral data helps improve monitoring accuracy of soil salinity. Considering soil salinity prediction accuracy and model complexity, $R^{1/2}$ transformation not only has higher verification accuracy (the model verification accuracy R^2(V) is increased from 0.1751~0.2786 in the original spectral index model to 0.4351~0.6472), but also achieves the highest prediction accuracy when fewer factors (n=10) are introduced to the model.

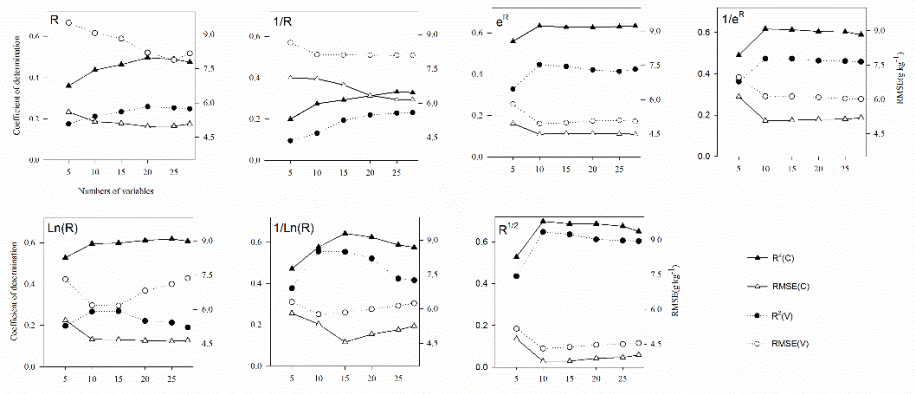

Figure 4 Influence of variable numbers to model reliability of PLSR model under 6 transformation

3.2.3 Optimization and verification of the estimation model

Based on the principle of maximum R^2(V) and minimum RMSE(V), the PLSR model with 10 factors of $R^{1/2}$ transform participating in modeling (R^2(V) is 0.6472 and RMSE(V) is 4.3106 is selected as the optimal model. It can be seen that a good linear relationship is shown between the predicted value and the measured value as a whole. Most samples are distributed on both sides of the 1:1 line. However, some samples deviate from the 1:1 line, and measured salt mass fraction between 0~10 g kg^{-1} inverse values between 7~12 g kg^{-1}, which are higher than the measured value.

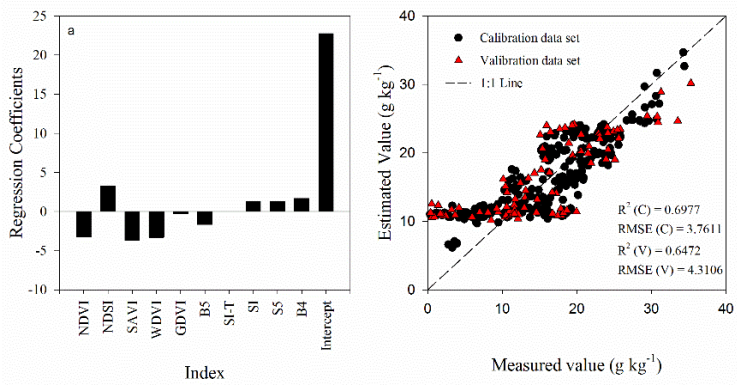

Figure 5 The coefficient of optimal model and verification (10 variables of PLSR model under $R^{1/2}$ transformation)

3.3 Remote sensing inversion of soil salinity

The optimal model of this study was applied to remote sensing images, and the soil salt content distribution map of Manas River Basin was obtained by inversion (Figure 6). Most of the farmland soil in the study area belongs to moderate and severe salinized soil, accounting for 58.97% and 25.41% of farmland in the irrigation area of Manas River, respectively. The areas with severe soil salinization are mainly located in the southeast of Manas River Basin, which is mainly because the area is located at alluvial-proluvial fan edge of the basin, with shallow burial depth of groundwater and unsmooth flow, and the soil texture is mainly clay loam with high salt content.

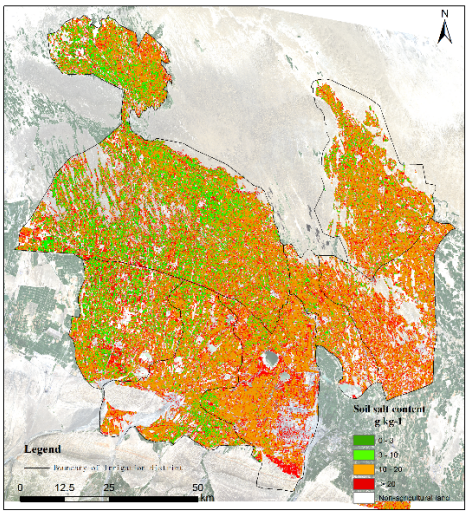

Figure 6 Inversion of soil salinity content in Manas River Basin

4 Conclusion

In this paper with Xinjiang Manas River Basin as the research area, a quantitative estimation model of soil salinity is constructed by integrating field measured data, Landsat8 remote sensing data and vegetation, soil and water spectral index groups. The conclusions are drawn as follows:

(1) There is low correlation between the reflectance of original band of Landsat satellite image, with the highest in B10 band (0.3689). Logarithmic transformation Ln(R), exponential transformation e^R and square root transformation $R^{1/2}$ of the spectral group data significantly improve the correlation between soil salinity and various indexes. Where, transformation form with the most significant increase is $R^{1/2}$, with a maximum increase of S5, which is increased by 0.4510 compared with the original correlation coefficient, indicating that spectral transformation is an effective way to improve the correlation between spectral index and salt content.

(2) In comparison of the three methods of PLSR, PCR and MLR for constructing soil salt estimation model, based on all spectral index modeling, PLSR model is the best, followed by PCR model and MLR model is the worst.

(3) By adding the spectral group index of the seven data transformation forms to the PLSR model from big to small according to the absolute value of the correlation coefficient, it is found that except 1/R transformation, stability of the other six transformational models first increases and then decreases as the number of factors increases. Finally, according to the principle of maximum R^2(V) and minimum RMSE(V), the PLSR model with 10 factors of $R^{1/2}$ transformation participating in modeling is selected as the optimal interpretation model for soil salinity (R^2 (V) is 0.6472 and RMSE (V) is 4.3106 g kg^{-1}).

REFERENCES

Allbed, A. , Kumar, L. , & Aldakheel, Y. Y. . (2014). Assessing soil salinity using soil salinity and vegetation indices derived from ikonos high-spatial resolution imageries: applications in a date palm dominated region. Geoderma, 230-231, pp. 1-8.

BAO Shi-dan. (2010). Analysis of agrochemical soil. Third Edition. Beijing:China Agricultural Press, pp. 25-114.

Fernandez-Buces, N., Siebe, C., Cram, S., & Palacio, J. L. (2006). Mapping soil salinity using a combined spectral response index for bare soil and vegetation: A case study in the former lake Texcoco, Mexico. Journal of Arid Environments, 65(4), pp. 644-667.
Hao, Y. , Mingyue, L. , Baojia, D. , Zongming, W. , Liangjun, H. , & Bai, Z. . (2018). Mapping soil salinity/sodicity by using landsat oli imagery and plsr algorithm over semiarid west jilin province, china. Sensors, 18(4), pp. 1048-.
Jibo, Y. , Haikuan, F. , Guijun, Y. , & Zhenhai, L. . (2018). A comparison of regression techniques for estimation of above-ground winter wheat biomass using near-surface spectroscopy. Remote Sensing, 10(1), pp. 66.
Kertész, M., & Tóth, T. (1994). Soil survey based on sampling scheme adjusted to local heterogeneity. Agrokémia és Talajtan, 43(1–2), pp. 113-132.
Metternicht, G. I., & Zinck, J. A. (2003). Remote sensing of soil salinity: potentials and constraints. Remote sensing of Environment, 85(1), pp. 1-20.
Peng, J., Biswas, A., Jiang, Q., Zhao, R., Hu, J., Hu, B., & Shi, Z. (2019). Estimating soil salinity from remote sensing and terrain data in southern Xinjiang Province, China. Geoderma, 337, pp. 1309-1319.
Peñuelas, J., Isla, R., Filella, I., & Araus, J. L. (1997). Visible and near-infrared reflectance assessment of salinity effects on barley. Crop science, 37(1), pp. 198-202.
Shao, J. L., & Cui. (2003). Study on groundwater resource analyses and development in manas plain. Arid Land Geography.
Shi, T., Chen, Y., Liu, Y., & Wu, G. (2014). Visible and near-infrared reflectance spectroscopy—An alternative for monitoring soil contamination by heavy metals. Journal of hazardous materials, 265, pp. 166-176.
Shrivastava, P., & Kumar, R. (2015). Soil salinity: a serious environmental issue and plant growth promoting bacteria as one of the tools for its alleviation. Saudi journal of biological sciences, 22(2), pp. 123-131.
The National Soil Survey Office. Soils of China. Beijing: China Agriculture Press, 1998.
Wang, F., Chen, X., Luo, G., & Han, Q. (2015). Mapping of regional soil salinities in Xinjiang and strategies for amelioration and management. Chinese geographical science, 25(3), pp. 321-336.
Wang, H., & Jia, G. (2012). Satellite-based monitoring of decadal soil salinization and climate effects in a semi-arid region of China. Advances in Atmospheric Sciences, 29(5), pp. 1089-1099.
Wang, Z. H. , He, X. L. , Yang, G. , & Li, S. . (2010). Sustainable strategies and status of unconventional water resources development and utilization in manas river basin. Advanced Materials Research, 113-116, pp. 565-570.